DOI: 10.1002/ejic.200801083

Oligonucleotide Duplexes with Tethered Photoreactive Ruthenium(II) Complexes: Influence of the Ligands and Their Linker on the Photoinduced Electron Transfer and Crosslinking Processes of the Two Strands

Stéphanie Deroo,[a] Stéphane Le Gac,[a] Sumana Ghosh,[b] Mathilde Villien,[b] Pascal Gerbaux,[c] Eric Defrancq,[b] Cécile Moucheron,[a] Pascal Dumy,[b] and Andrée Kirsch-De Mesmaeker*[a]

Keywords: Conjugation / DNA damage / Oligonucleotides / Ruthenium / Electron transfer

The photoreactivity of new Ru^{II}-oligonucleotide conjugates is investigated in the presence of their complementary strands. The goal is to determine the origins of different effects of parameters that control the photocrosslinking process of the two strands. Therefore, two Ru^{II} compounds, either $[Ru(tap)_3]^{2+}$ or $[Ru(tap)_2phen]^{2+}$ (tap = 1,4,5,8-tetraazaphenanthrene, phen = 1,10-phenanthroline) with different oxidation powers, were tethered with different linkers to either the 5′- or 3′-phosphate end of the probe strand before hybridization with the complementary strand. These systems were studied by time-resolved emission spectroscopy, UV/Vis absorption experiments, PAGE and MS (ESI) analyses. The best yields of photocrosslinking (45%) obtained with $[Ru(tap)_3]^{2+}$ tethered to the 3′-position are due to (i) a higher oxidation power of the complex and (ii) its attachment at the 3′-position. Indeed, this tethering favours the interaction of the Ru compound with the duplex and, therefore, inhibits its photodechelation. This work allows better design of sequence-specific DNA photodamaging agents prior to biological applications.

Introduction

Antisense oligonucleotides (ODNs) represent interesting therapeutic candidates for the repression of gene expression. They could inhibit specifically the synthesis of a particular protein by binding to its encoding mRNA (antisense strategy).[1] Applications using this strategy have already emerged; for example, an antisense ODN is presently used to treat retinal necrosis due to human cytomegalovirus and other ODNs are currently in clinical trials.[2,3] Nevertheless, this conceptually simple approach for gene expression inhibition encounters several obstacles. Among others, antisense ODNs are sensitive to degradation by nucleolytic enzymes[4,5] and their negative charges prevent them from crossing cell membranes.[6,7] Various chemical modifications have been developed to enhance their nuclease resistance and numerous delivery systems are studied nowadays.[8,9] To improve cellular penetration, hydrophobic substances, peptidic vectors or molecules that are substrates of internalization receptors have been tethered to ODNs.[10,11] Nucleic acid damaging agents have also been attached to ODNs to inhibit the expression of a specific mRNA.[12]

In this frame of research, we have been interested in the coupling of ruthenium(II) complexes to ODNs. We previously demonstrated that Ru^{II} complexes containing at least two π-deficient polyazaaromatic ligands such as tap (1,4,5,8-tetraazaphenanthrene) are able to form a photoadduct on the guanine (G) base of DNA or ODN and can also photocleave plasmidic DNA.[13,14] These reactions are induced by a photoelectron transfer process from the G base to the excited complex.[15] We have shown that formation of the photoadduct could be targeted towards a G residue of a specific sequence by using ODNs conjugated with the $[Ru(tap)_2dip]^{2+}$ complex (dip = 4,7-diphenylphenanthroline).[16] In this case, the photoreaction leads to efficient crosslinking of the ruthenium derivatized ODN with its complementary strand (respectively, the probe and the target strands; Figure 1).[16a] With in vitro systems, this photodamage blocks the activity of a 3′-exonuclease with 100% efficiency and stops the elongation of a DNA primer by two different DNA polymerases.[16] Although these Ru–ODN conjugates have allowed much information to be gained with regard to the reaction steps that lead to photocrosslinking, there are several factors that prevent the devel-

[a] Chimie Organique et Photochimie CP160/08, Université libre de Bruxelles,
50 avenue F.D. Roosevelt, 1050 Bruxelles, Belgium
Fax: +32-26503018
E-mail: akirsch@ulb.ac.be
[b] Département de Chimie Moléculaire UMR CNRS 5250, Université Joseph Fourier,
301 rue de la Chimie BP53, 38041 Grenoble Cedex 9, France
[c] Laboratoire de Chimie Organique, Centre de Spectrométrie de Masse, Université de Mons-Hainaut,
19 avenue Maistriau, 7000 Mons, Belgium

Supporting information for this article is available on the WWW under http://www.eurjic.org or from the author.

opment of the systems described in Figure 1 for further applications. First of all, the amide-based coupling procedure for the attachment of $[Ru(tap)_2dip]^{2+}$ to the ODNs required as many as 100 equivalents of derivatized complex, the synthesis of which, moreover, was not straightforward. Poor yields of conjugates (maximum 20%) were obtained.

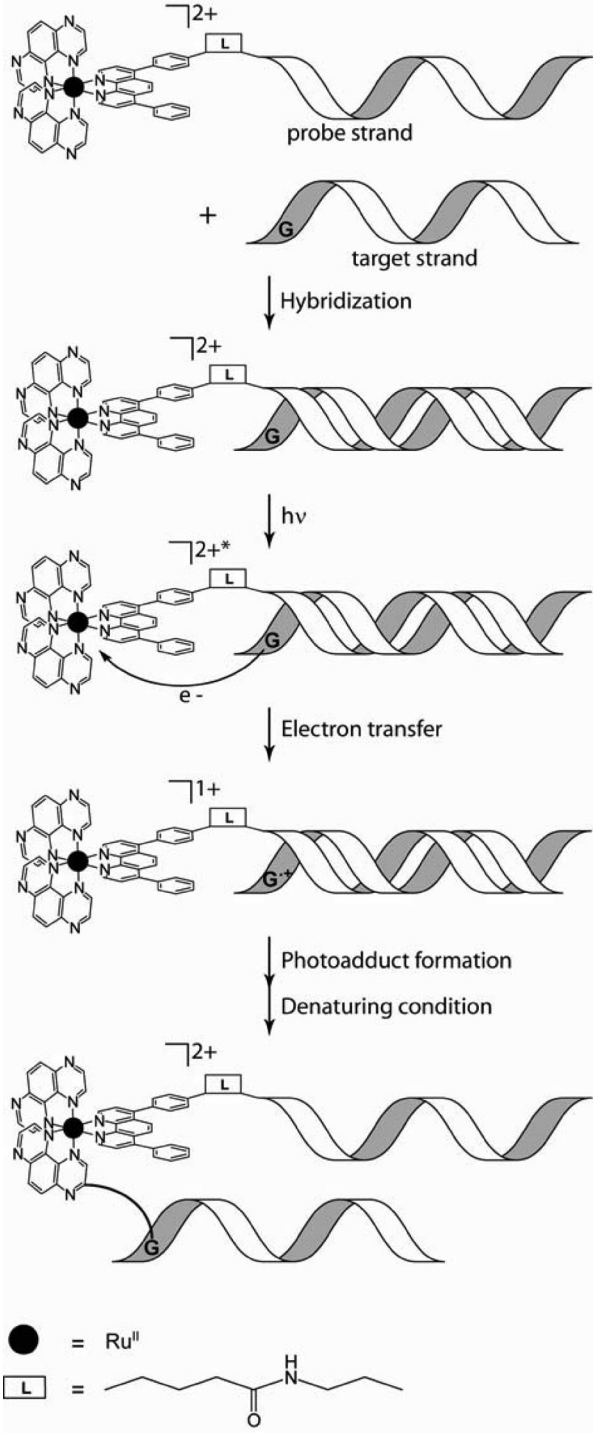

Figure 1. Schematic representation of the photocrosslinking process with the previously studied $[Ru(tap)_2dip]^{2+}$.

During the last decade, great efforts have been devoted to new methods for the efficient incorporation of reporters into oligonucleotides and have resulted in the development of the concept of "click chemistry".[17] Among the various proposed strategies, Huisgen's cycloaddition has received particular attention, as the involved functional groups have shown good compatibility with DNA synthesis.[18] However, this strategy involves copper catalysis, which complicates the conjugation with metal moieties such as ruthenium complexes. Thus, we adapted a novel tethering procedure, initially developed for the chemoselective ligation of ODNs with carbohydrates, peptides and glycopeptides[19] and which also fulfilled the criteria of click chemistry. It proceeds by the condensation reaction of the aminooxy-derivatized Ru^{II} complex with an aldehyde containing ODN either at the 3′- or 5′-extremity leading to an oxime linkage (Figure 2) with good and reproducible yields (about 40%).[20]

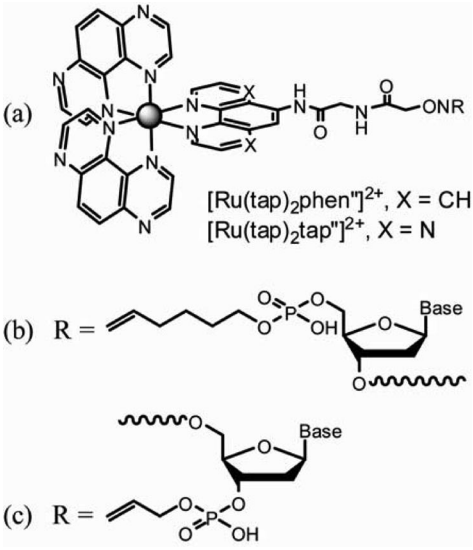

Figure 2. (a) Derivatized complexes and anchoring at the 5′- (b) and 3′-extremity (c) of the oligonucleotide, where "base" represents the first nucleic residue.

With these new Ru–ODN conjugates in hand, the study of their photochemical behaviour, in particular in the presence of G-containing ODN targets, is a prerequisite for their further use in biological assays (i.e., for gene expression inhibition). The goal of the present work is to evaluate, with different techniques, the importance and origin of the effects of several parameters on the photoelectron transfer and photocrosslinking yield. Thus, the influence of the nature of the tethered ruthenium complex, $[Ru(tap)_2phen]^{2+}$ versus $[Ru(tap)_3]^{2+}$ (with different oxidation powers), the linker and its site of attachment on the ODN, the 3′- versus 5′-extremity (Figure 2) have been considered. The "rules" for photocrosslinking resulting from this study could thus afterwards be applied in biological assays.

Results and Discussion

Several parameters may influence both the photoinduced electron transfer and the photocrosslinking processes. First,

as a result of the different precursors used for the 3′- and 5′-aldehyde incorporation into the oligonucleotides, the linker is longer when attached at the 5′-position than at the 3′-position (Figure 2, b vs. c). This might induce a difference in the interaction of the complexes with the hydrophobic grooves of the duplexes. Secondly, the use of excited $[Ru(tap)_3]^{2+}$ should cause two antagonistic effects. Because of its higher oxidation power (E^*_{red} = +1.30 V as compared to +1.15 V vs. SCE for $[Ru(tap)_2phen]^{2+}$) $[Ru(tap)_3]^{2+}$ should lead to a more efficient photoelectron transfer, but because of its more important crossing from the ^{3}MLCT to the ^{3}MC excited state, its photodechelation could be favoured. To examine these different parameters, eight duplexes, shown in Table 1, were designed. Two target sequences with or without guanine residues, named 1 or 0, respectively, were chosen. Sequence 0 was selected as a reference, as it should not lead to luminescence quenching and photocrosslinking between the two strands. Sequence 1, with a GG track close to the attachment site of the Ru compound on the probe strand, was chosen on the basis of our expertise gained with the $[Ru(tap)_2dip]^{2+}$ conjugates in order to get a high percentage of photocrosslinking. The $[Ru(tap)_2phen"]^{2+}$ and $[Ru(tap)_2tap"]^{2+}$ complexes were tethered as indicated above to either the 5′- or 3′-extremity of the probe sequences 0 and 1, thus leading to the eight duplexes shown in Table 1 (for their characterization by mass spectrometry, see the Experimental Section).

Table 1. The different Ru–ODNs duplexes and the corresponding abbreviations. The anchored complex, the ODN extremity of tethering and the sequence are shown. The guanine bases in the complementary strand are highlighted in italics.

Abbrev.	Complex–duplex	
RuT_2P-5′-0	$[Ru(tap)_2phen"]^{2+}$-	5′-TTT TTT TAT TAA ATT TA-3′ 3′-AAA AAA ATA ATT TAA AT-5′
RuT_2P-5′-1	$[Ru(tap)_2phen"]^{2+}$-	5′-TCC TTT TAT TAA ATT TA-3′ 3′-A*GG* AAA ATA ATT TAA AT-5′
RuT_2P-3′-0	$[Ru(tap)_2phen"]^{2+}$-	3′-TTT TTT TAT TAA ATT TA-5′ 5′-AAA AAA ATA ATT TAA AT-3′
RuT_2P-3′-1	$[Ru(tap)_2phen"]^{2+}$-	3′-TCC TTT TAT TAA ATT TA-5′ 5′-A*GG* AAA ATA ATT TAA AT-3′
RuT_3-5′-0	$[Ru(tap)_2tap"]^{2+}$-	5′-TTT TTT TAT TAA ATT TA-3′ 3′-AAA AAA ATA ATT TAA AT-5′
RuT_3-5′-1	$[Ru(tap)_2tap"]^{2+}$-	5′-TCC TTT TAT TAA ATT TA-3′ 3′-A*GG* AAA ATA ATT TAA AT-5′
RuT_3-3′-0	$[Ru(tap)_2tap"]^{2+}$-	3′-TTT TTT TAT TAA ATT TA-5′ 5′-AAA AAA ATA ATT TAA AT-3′
RuT_3-3′-1	$[Ru(tap)_2tap"]^{2+}$-	3′-TCC TTT TAT TAA ATT TA-5′ 5′-A*GG* AAA ATA ATT TAA AT-3′

The Free Complexes

The effect of the linker on the photophysical properties of the free complexes was first examined. No significant differences are observed either in the absorption or the emission maxima between the aminooxy-derivatized complexes and their related compounds (Table 2, Entries 1–4). The emission lifetimes are slightly more important when the complexes are functionalized by the linker, as already observed previously in other cases of derivatization.[21] Their photostability was also examined. Indeed, whereas $[Ru(tap)_2phen]^{2+}$ is stable under illumination, for $[Ru(tap)_3]^{2+}$ it was shown that as a result of its high percentage of thermal activation from the ^{3}MLCT to the ^{3}MC state, it can undergo loss of one of the ligands, which results in photosubstitution.[22] This process can be monitored by recording UV/Vis absorption spectra in which the MLCT band at 400 nm is bleached upon irradiation and is replaced by a new band around 500 nm, with a characteristic isosbestic point at 450 nm. Absorption in the 500 nm region is typical of $[Ru^{II}(tap)_2XY]^{n+}$ (X and Y are H_2O or Cl^-).[22] To check whether the functionalization of the complex could modify this photodechelation process, the changes in the UV/Vis spectra of $[Ru(tap)_2phen"]^{2+}$ and $[Ru(tap)_2tap"]^{2+}$

Table 2. Spectroscopic data for the Ru-ODN duplexes and the corresponding free complexes.

Entry	Sample	Abs.	Em.[b]	Excited-state lifetimes[d]								
		λ_{max} (nm)[a]	λ_{max} (nm)[a,c]	τ_0 (ns)	A_0 (%)	τ_1 (ns)	A_1 (%)	τ_2 (ns)	A_2 (%)	τ_3 (ns)	A_3 (%)	τ_m (ns)[e]
1	$[Ru(tap)_2phen"]^{2+}$	412, 460	649	720	100	–	–	–	–	–	–	–
2	$[Ru(tap)_2phen]^{2+}$[f]	410, 466	645	690	100	–	–	–	–	–	–	–
3	$[Ru(tap)_2tap"]^{2+}$	407, 436	599	226	100	–	–	–	–	–	–	–
4	$[Ru(tap)_3]^{2+}$[g]	408, 437	602	220	100	–	–	–	–	–	–	–
5	RuT_2P-5′-0	416, 463	645	–	–	–	–	720	49	1410	51	1070
6	RuT_2P-5′-1	416, 463	646	–	–	96	51	420	32	1055	17	360
7	RuT_3-5′-0	408, 439	610	–	–	195	53	570	41	1775	6	445
8	RuT_3-5′-1	408, 442	600	–	–	69	42	295	51	1345	7	275
9	RuT_2P-3′-0	416, 463	645	–	–	–	–	755	56	1720	44	1180
10	RuT_2P-3′-1	415, 463	653	–	–	56	45	270	45	955	10	245
11	RuT_3-3′-0	409, 438	597	–	–	138	47	355	48	1183	5	294
12	RuT_3-3′-1	408, 441	598	–	–	22	77	180	20	750	3	75

[a] Experimental error ±2 nm. [b] Excitation at wavelength maxima of the MLCT band: 416 nm for the $[Ru(tap)_2phen]^{2+}$ systems and 408 nm for the $[Ru(tap)_3]^{2+}$ systems. [c] The emission maxima were corrected for the photomultiplier response. [d] Luminescence decays monitored at 645 nm for the $[Ru(tap)_2phen]^{2+}$ systems and at 600 nm for the $[Ru(tap)_3]^{2+}$ systems (λ_{exc} = 379 nm) analyzed according to a multiexponential function: $I_{em}(t) = \Sigma_i a_i \exp(-t/\tau_i)$ with i = 1, ...; the normalized preexponential factors ($A_i = a_i/\Sigma a_i$) reflect the contributions of the different decay components to initial emission. The experimental errors are the standard deviations estimated from at least three different measurements; for biexponential fittings ±10%; triexponential fittings ±10% for τ_3, ±15–20% for τ_1 and τ_2. [e] Preexponential weighted mean lifetime, $\tau_m = (\Sigma a_i\tau_i)/(\Sigma a_i)$. [f] See ref.[2] [g] See ref.[22]

under irradiation were monitored (see Figure S1 in the Supporting Information, A and B, respectively). It turned out that no effect of the derivatization was observed, as $[Ru(tap)_2tap"]^{2+}$ photodechelates like its non-derivatized counterpart (isosbestic point at 450 nm), whereas $[Ru(tap)_2phen"]^{2+}$ was insensitive to light irradiation. The dechelation of $[Ru(tap)_2tap"]^{2+}$ in the excited state (or photodegradation) should thus represent a drawback for the subsequent photoadduct formation.

Table 3. Percentages of quenching from emission lifetime and intensity measurements for the RuT_2P duplexes of sequence 1.[a]

	$\%Q = 1 - I/I_0$[b]	$\%Q = 1 - \tau_m/\tau_{m0}$[c]
RuT_2P-5′-1	60 ± 2	63 ± 2
RuT_2P-3′-1	82 ± 2	79 ± 2

[a] Experimental errors: estimated from at least three different measurements. [b] I and I_0 are the luminescence intensities of the duplexes of sequence 1 (i.e., RuT_2P-5′-1 and RuT_2P-3′-1) and sequence 0 (i.e., RuT_2P-5′-0 and RuT_2P-3′-0), respectively. [c] Similarly, τ_m and τ_{m0} are the weighted average lifetimes for the duplexes with and without quenching (respectively, sequence 1 and 0).

5′-Ru^{II} Metallated Duplexes

Analysis of the Luminescence Decay Profiles Under Pulsed Illumination

The comparison of the emission lifetimes of each duplex will afford pieces of information on the luminescence quenching by the G bases and on the possible protection of the excited complex by the other bases of the double helix.

The emission decay profiles of the double-stranded Ru^{II} ODNs were fitted to multiexponential functions; the results are collected in Table 2 for air-equilibrated solutions (Table 2, Entries 5 to 8). The fact that the decays correspond to multiexponential functions indicates that several ODN microenvironments are probed by the attached excited complexes.[23] The comparison of the weighted average lifetimes $\tau_m = (\Sigma a_i\tau_i)/(\Sigma a_i)$[24] with the lifetimes of the free complexes indicates whether the average of the different populations of excited complexes undergoes protection or quenching by the duplex. On this basis, examination of Table 2 leads to the following information. For the duplex sequence 0 derivatized with $[Ru(tap)_2phen]^{2+}$ (i.e., RuT_2P-5′-0; Table 2, Entry 5), τ_m is longer than τ_0 of the free complex (Table 2, Entry 1); the long-lived component τ_3 (longer than that of the free complex) can be attributed to a population of luminophores protected from water by the hydrophobic ODN duplex. The second lifetime τ_2, close to that of the free excited complex, can be assigned to a non-protected species probably located in the polyphosphate backbone microenvironment. In the presence of guanine bases, sequence 1 (i.e., RuT_2P-5′-1; Table 2, Entry 6), τ_m is shorter than τ_0 and a triexponential function is necessary to fit the decay profiles. The long-lived component (τ_3) with a lower normalized preexponential factor (A_3) could be attributed to a small population of excited species that, thanks to the relatively long linker, are too far away from the GG track to be quenched. The shortest lifetime (τ_1) with the highest percentage of contribution (51%) reflects the participation of G-quenched excited states. To determine whether among these quenching processes some are static, the comparison of the quenching measurements from the emission lifetimes under pulsed illumination ($\%Q = 1 - \tau_m/\tau_{m0}$) and from the emission intensities under steady-state illumination ($\%Q = 1 - I/I_0$) was made (Table 3).[24] Within experimental error, the ratios in luminescence intensity and lifetime are the same (≈60%). Consequently, no static quenching is involved in the luminescence inhibition process for this complex.

The behaviour of $[Ru(tap)_3]^{2+}$ attached to the duplexes is different. Indeed, the luminescence decay profile for the RuT_3-5′-0 duplex (Table 2, Entry 7) needs a triexponential function to be fitted, although no G base is present and τ_m is longer than τ_0. Surprisingly, the lifetime component with the highest contribution (195 ns, 53%) is slightly shorter than that of the free complex (226 ns under air; Table 2, Entry 3). Therefore, this might reflect the presence of a modest luminescence quenching by the adenine (A) residues. A previous study of the system $[Ru(tap)_3]^{2+}$ and AMP (adenosine-5′-monophosphate) had shown indeed the presence of a slight quenching of luminescence intensity and lifetime of the excited complex, with a kinetic quenching constant k_q of about 0.12×10^9 $M^{-1}s^{-1}$.[15] Thus, the track of adenine residues in the complementary strand facing the Ru^{II} complex can be responsible for this slight quenching. In contrast, as in the case of the $[Ru(tap)_2phen]^{2+}$ conjugate, longer emission components participate also to the decay process. In this case, in addition to the factors mentioned above for this effect, the lengthening could also be due to a decrease in the thermal activation of the ^{3}MLCT to the ^{3}MC state of attached $[Ru(tap)_3]^{2+}$ caused by the imprisonment of the complex by the double helix.

In the case of RuT_3-5′-1 (Table 2, Entry 8), a triexponential function is again needed to fit the decay profile because of important quenching not only by the A bases but mainly by the G units. The value of τ_m is indeed shorter than the corresponding value without G bases (275 vs. 445 ns), and the short component τ_1 is also shorter for sequence 1 than 0 (69 vs. 195 ns; Table 2, Entry 8 vs. 7). However, there is still a slight contribution of a long-lived component, which indicates that a certain population of excited species does not interact at the level of the G bases.[25,26]

Detection of Photoadduct Formation (i.e., Photocrosslinking) by Absorption Measurements

As already mentioned, the luminescence quenching evidenced by the emission measurements can be attributed to a photoinduced electron transfer. Afterwards, by recombination of the so-produced radical species (monoreduced complex and monooxidized G unit) a photoadduct can be formed at the level of the G bases. Its formation can be assessed by modifications of the UV/Vis absorption spectra as a function of the illumination time of the duplexes.[16]

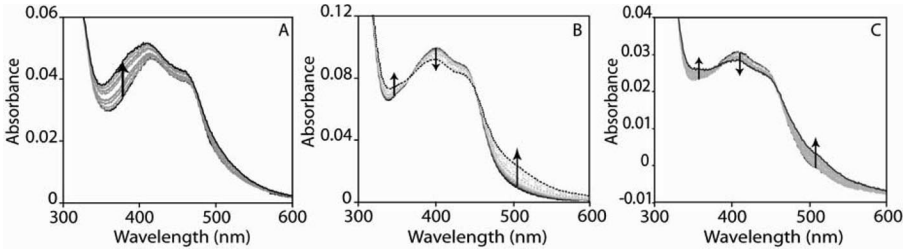

Figure 3. Absorption spectra of the RuT_2P-5′-1 (A), RuT_3-5′-0 (B) and RuT_3-5′-1 (C) duplexes after visible irradiation, up to 120 min, in aqueous buffer solution at pH 7, 50 mM NaCl, 10 mM Tris-HCl.

Whereas the absorption spectrum of the RuT_2P-5′-0 duplex is unaffected (data not shown) upon illumination, a clear hyperchromic effect around 350 nm, with a slight shift of the maximum to shorter wavelengths (Figure 3A) is observed for the RuT_2P-5′-1 duplex. This effect may be attributed to the formation of photoadducts on one of the two G bases of the complementary strand. In contrast, steady-state illumination of the RuT_3-5′-0 duplex leads to a decrease in the MLCT band, with an increase around 500 nm (isosbestic point around 450 nm) and a slight absorption increase at 350 nm (Figure 3B). The two first modifications are representative of the photodechelation process, but the hyperchromic effect at 350 nm could be due to photoreactions involving the A bases of the target strand. Interestingly, the same kind of modifications are observed on continuous irradiation of the RuT_3-5′-1 duplex (Figure 3C). This indicates that, with the highly oxidizing excited $[Ru(tap)_3]^{2+}$ complex, the photodechelation process competes importantly with the formation of photoadducts (with A or G bases), even when the Ru compound is facing GG bases.

Photocrosslinking Detected by Gel Electrophoresis

If the spectral changes around 350 nm indeed arise from formation of the photoadducts, and thus from photocrosslinking of the two strands, this process can be easily detected and quantified by polyacrylamide gel electrophoresis (PAGE) experiments under denaturing conditions by using radiolabelled oligonucleotides. Indeed, there will be an important difference in electrophoretic mobility between a 17-mer strand and a photocrosslinked duplex corresponding to a 34-mer.[16] For that purpose, the target strands were 5′-end ^{32}P labelled before hybridizing with the 5′-Ru–ODN probe. The Ru-metallated duplexes were thus illuminated for different times and analyzed by PAGE under denaturing conditions (Figure 4). Continuous illumination of the RuT_3-5′-1 and RuT_2P-5′-1 duplexes (respectively, lanes 2 to 5 and 12 to 15) leads in both cases to the formation of a retarded band, which migrates like a duplex and thus corresponds to covalent photocrosslinking of the two strands (see also further for mass spectrometry data). Irradiation of the RuT_2P-5′-0 duplex does not lead to formation of this species, whereas illumination of the RuT_3-5′-0 duplex shows the appearance of a similar very weak retarded band, accounting for less than 5% of the total radioactivity (data not shown). This latter could originate either from the formation of an adduct due to dechelation of the complex and rechelation with an adenine base or even from a photoadduct (as explained before for the G base) with an adenine base. The percentages of photocrosslinking have been quantified by radioactivity counting. Figure 5 shows the results for the RuT_2P-5′-1 and RuT_3-5′-1 duplexes as a function of the illumination time. Hence, these two systems lead to a ca. 30% yield of photocrosslinking after a 30 min illumination. A slight difference between the two complexes is ob-

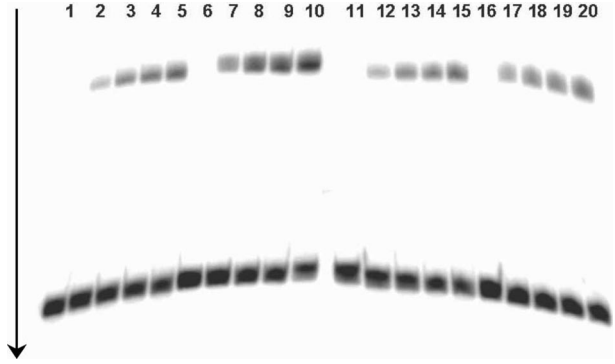

Figure 4. Autoradiogram of a 20% denaturing polyacrylamide gel showing the ^{32}P labelled duplexes, where the non-Ru-derivatized single-strand oligonucleotide (target strand) was 5′-end labelled. The reaction mixture contained 8 μM duplex in a total volume of 60 μL with 50 mM NaCl and 10 mM Tris-HCl (pH = 7). Each solution was illuminated by a 442 nm laser beam for a defined time period and an aliquot of 10 μL of the reaction mixture was analyzed for each time. Lanes 1–5 correspond to the RuT_3-5′-1 duplex illuminated for 0, 5, 10, 15 and 30 min. Likewise, RuT_3-3′-1 (lanes 6–10), RuT_2P-5′-1 (lanes 11–15) and RuT_2P-3′-1 (lanes 16–20) were illuminated for the same time periods.

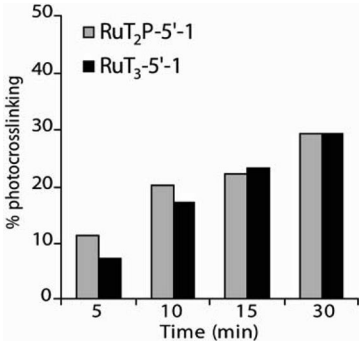

Figure 5. Percentages of photocrosslinking obtained with the RuT_2P-5′-1 and RuT_3-5′-1 duplexes with increasing illumination times (from PAGE experiments).

served for the short illumination times, which could be attributed to the dechelation process of the excited complex in RuT_3-5′-1, which competes with the electron transfer and consequently with the photocrosslinking of the two strands.

3′-Ru-Metallated Duplexes and Comparison with the 5′-Attachment

The same experiments as those for the attachment at the 5′ end of the ODN were carried out for tethering at the 3′-position. The length of the linker, which differs for attachment at the 3′- and 5′-positions (see Figure 2), could alter the behaviour of the two attached complexes.[27]

A comparison of the τ_m values for the 3′-attached $[Ru(tap)_2phen]^{2+}$ with the corresponding values for the 5′-tethered complex (Table 2) shows that (i) for sequence 0, the τ_m value is a bit longer at the 3′-position (Table 2, Entry 5 vs. 9) and (ii) for sequence 1, τ_m is slightly shorter at the 3′-position (Table 2, Entry 6 vs. 10). The results of this comparison clearly indicate that the excited metallic species $[Ru(tap)_2phen]^{2+}$ interacts slightly better with the duplex when it is attached at the 3′-position, that is, with a shorter linker, than at the 5′-position. Indeed, without guanine bases in the duplex, because of better protection, the mean averaged lifetime is increased, and with the G-containing duplex, because of more efficient electron transfer, the mean averaged lifetime is shortened. The more efficient interaction of the complex attached with the 3′-linker is also confirmed by a more important percentage of emission quenching for the 3′-attachment (≈80%) than for the 5′-attachment (≈60%), which is also due to dynamic quenching (Table 3).

For $[Ru(tap)_3]^{2+}$, the influence of the 3′- vs. 5′-tethering is also highlighted in Table 2. First, a comparison of the τ_m values and the shorter lifetimes (τ_1) for the RuT_3-3′-0 and RuT_3-5′-0 duplexes indicates that the quenching by the A bases is more important when $[Ru(tap)_3]^{2+}$ is anchored at the 3′-position than at the 5′-position (Table 2, Entry 11 vs. 7). Moreover, in the duplexes of sequence 1, the weighted averaged lifetime value τ_m is much shorter for $[Ru(tap)_3]^{2+}$ in the 3′-position than in the 5′-position (75 vs. 275 ns; Table 2, Entry 12 vs. 8). This indicates a much more efficient electron transfer process in the 3′-position than in the 5′-position with the G units. This important difference between the two attachment positions suggests of course that the complex is closer to the GG track when tethered in 3′-position.

The efficiency of luminescence quenching (or light-induced electron transfer) correlates also with the photoadduct formation as detected by absorption spectroscopy. As shown by comparison of Figures 4 and S2 (Supporting Information), more photoproduct is formed when the $[Ru(tap)_2phen]^{2+}$ or $[Ru(tap)_3]^{2+}$ complex is anchored to the 3′-end than to the 5′-end of the ODN (Figure S2, C and D; Supporting Information). More interestingly, the typical spectral feature of the photodechelation process (isosbestic point around 450 nm) is not detected for the RuT_3-3′-1 duplex (Figure S2, B; Supporting Information). This indicates that when $[Ru(tap)_3]^{2+}$ is anchored with the shorter linker at the 3′-end of the ODN, in addition to better photoadduct formation (photocrosslinking of the strands), the photodechelation process seems to be suppressed. This absence of photodechelation of $[Ru(tap)_3]^{2+}$ attached to the 3′-end in a duplex was checked with the ^{32}P labelled RuT_3-3′-1 in single strand and in duplex form by PAGE analysis. Thus, illumination of the single strand (Figure 6, lanes 1 to 5) reveals the presence of photodechelated product (which migrates slightly faster than that of the starting single strand ODN), and which increases with the illumination time. Only trace amounts of this photodechelated product were detected with the same RuT_3-3′-1 ODN in the duplex form under illumination (Figure 6, lanes 6 to 10). These observations are in favour of the fact that when the ^{3}MLCT state of $[Ru(tap)_3]^{2+}$ has no electron donor in its close vicinity (absence of G units), it photodecomposes by the loss of a ligand (i.e., the chemically attached and/or a non-chemically attached tap).

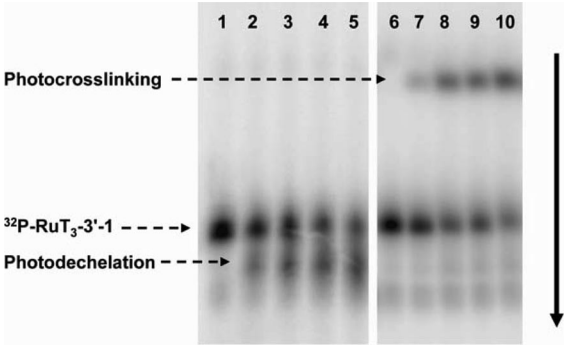

Figure 6. Autoradiogram of a 20% denaturing polyacrylamide gel showing the ^{32}P-5′ end labelled 17-mer RuT_3-3′-1 as single strand (Lanes 1–5) and double strand (lanes 6–10) as a function of the illumination time. The reaction mixture contained single-strand oligonucleotide or duplex (8 μM) in a total volume of 60 μL in 50 mM NaCl and 10 mM Tris-HCl (pH = 7) buffer solution. The solutions were illuminated by a 442 nm laser beam for a defined time period and an aliquot of 10 μL of the reaction mixture was analyzed for each time. Lanes 1–5 (and lanes 6–10) correspond to 0, 5, 10, 15 and 30 min of illumination, respectively.

Consequently, on the basis of the suppression of photodechelation of $[Ru(tap)_3]^{2+*}$ when attached to the 3′-end of duplex sequence 1 (shorter linker), we should conclude that the process in competition with this photodechelation, that is the electron transfer process, wins the competition. The photocrosslinking should thus become very efficient with the RuT_3-3′-1 duplex. Indeed, very interestingly, the comparison of the percentages of photocrosslinking (results from Figure 5) for the different duplexes indicates that the yield of this process with the attached $[Ru(tap)_3]^{2+}$ is not only higher when it is attached to the 3′-position than to the 5′ position (Figure 7A, ca. 45 vs. ca. 30%, respectively) but is even better than with $[Ru(tap)_2phen]^{2+}$ also attached to the 3′-position (Figure 7B, ca. 45 vs. ca. 25% for RuT_3-3′-1 and RuT_2P-3′-1, respectively). This can be reasonably well explained. The steric hindrance due to the double helix around the ^{3}MLCT state of the 3′-attached $[Ru(tap)_3]^{2+}$ in-

creases its lifetime as well as the barrier to reach the ^{3}MC state, so that the probability to be quenched by electron transfer from the GG track is also increased as well as the percentage of photocrosslinking. Consequently, for the investigated duplexes, in spite of an important dechelation process for the free $[Ru(tap)_3]^{2+}$ or to a lower extent for the 5′-tethered $[Ru(tap)_3]^{2+}$ in single or double strand, because of its higher oxidation power, this complex becomes more efficient than $[Ru(tap)_2phen]^{2+}$ to the condition that it is attached to the duplex in the 3′-position (shorter linker).

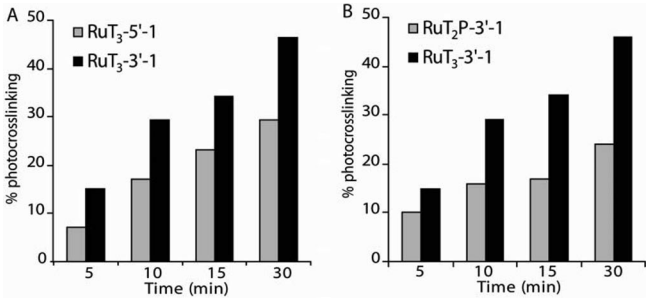

Figure 7. Comparison between the percentages of photocrosslinking with increasing illumination times for the RuT_3-5′-1 and RuT_3-3′-1 duplexes (A) and for the RuT_2P-3′-1 and RuT_3-3′-1 duplexes (B) (from PAGE experiments).

Characterization of the Photocrosslinked RuT_3-3′-1 Duplex

In addition to gel electrophoresis experiments, the occurrence of the photocrosslinking reaction was also investigated by nano-electrospray (nano-ESI) mass analyses. The RuT_3-3′-1 duplex, which gives the highest yield of photocrosslinking, was selected for those measurements. Actually, the photocrosslinking upon irradiation of the RuT_3-3′-1 duplex should correspond to the loss of a molecule of hydrogen resulting from the formation of the covalent bond. As a consequence, mass spectrometry confirmation of such a process should rely on the determination of a difference of 2 mass units between the non-irradiated and the irradiated duplexes. In other words, the mass spectra of the RuT_3-3′-1 duplex with and without illumination should be compared. However, because the photocrosslinking in this duplex is very efficient, it was difficult to obtain a sample with no photoreaction at all for the mass analysis. Moreover, the required mass accuracy for this kind of measurements is difficult to achieve. Indeed, we have to identify a 2 u difference out of 12000 u for a multiply charged species (sevenfold charged species as presented hereafter).

Therefore, as an alternative strategy, we decided to measure the nano-ESI mass spectrum of the illuminated RuT_3-3′-1 duplex sample under denaturing conditions (CH_3CN/H_2O, 1:1; 5 mM $AcO^-NH_4^+$ buffer). Actually, under these conditions, interactions, such as those existing in the non-irradiated duplex, are likely to be destroyed, in contrast to the covalent bond formation, which should characterize the illuminated duplex. Therefore, as a control for this study, we first measured the nano-ESI mass spectrum of a solution of the RuT_2P-3′-0 duplex under such conditions. As presented in Figure S3 (Supporting Information) and as expected, because this duplex cannot undergo a photocrosslinking process, no signal was detected for the intact RuT_2P-3′-0 duplex. However, ionic species related to both single strands were readily identified in the recorded spectrum.

In contrast, the mass spectrum obtained under denaturing conditions for the illuminated RuT_3-3′-1 duplex revealed, in addition to the corresponding single strands, the presence of a third species detected at m/z = 1610.5 (Figure 8). The corresponding ions are identified as sevenfold charged species. The comparison between the experimental data and three isotopic pattern simulations for the following ions, respectively (a) $[RuT_3\text{-}3'\text{-}1 - H_2 + 5H^+]$, (b) $[RuT_3\text{-}3'\text{-}1 - H_2 + 4H^+ + Na^+]$ and (c) $[RuT_3\text{-}3'\text{-}1 - H_2 + 3H^+ + 2Na^+]$, unambiguously confirms that the observed signals correspond to ions derived from the intact RuT_3-3′-1 duplex, in which both strands are covalently bound to each other.

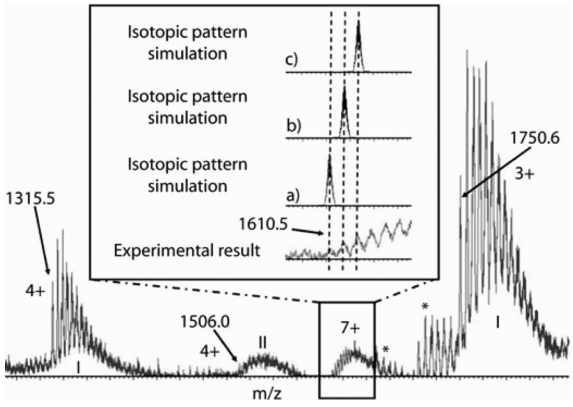

Figure 8. Mass spectrometry analysis of the crude illuminated solution of the RuT_3-3′-1 duplex: nano-ESI mass spectrum (positive ion mode) under denaturing conditions (see Experimental Section). Both separated single-strand oligonucleotides are detected in the mass spectrum as multiply charged cations (I: complementary strand, II: metallated strand). The signal observed at m/z = 1610.5 corresponds to a sevenfold charged species from the photocrosslinked RuT_3-3′-1 duplex $[RuT_3\text{-}3'\text{-}1 - H_2]$. The inset presents the comparison between the experimental result and three simulations of the isotopic pattern for the sevenfold charged photocrosslinked RuT_3-3′-1 duplex: (a) $[RuT_3\text{-}3'\text{-}1 - H_2 + 5H^+]$, $[RuT_3\text{-}3'\text{-}1 - H_2 + 4H^+ + Na^+]$ and (c) $[RuT_3\text{-}3'\text{-}1 - H_2 + 3H^+ + 2Na^+]$. Signals marked with an asterisk correspond to In-Source CID fragment ions (collision-induced dissociation - base losses).

Conclusions

The anchoring of the $[Ru(tap)_2phen]^{2+}$ and $[Ru(tap)_3]^{2+}$ complexes by using an efficient tethering method enabled the influence of the nature of the Ru complexes and the site of attachment (3′- vs. 5′-positions) on the photoinduced electron transfer as well as on the photoadduct formation to be investigated. For the $[Ru(tap)_3]^{2+}$ conjugates, the particular properties of the complex play different roles in the ODN duplex. Despite its high photooxidizing power, when the linker is too long (5′-attachment), the light-induced dechelation process competes efficiently with the photo-

crosslinking, which of course decreases. More interestingly, when the linker is short enough to allow better interaction of the complex with the ODN duplex (3′-attachment), the photodechelation process is suppressed and the photocrosslinking yield reflects the higher oxidizing power of the excited $[Ru(tap)_3]^{2+}$ relative to that of excited $[Ru(tap)_2phen]^{2+}$. This latter result is obviously of great interest for biological applications, as 3′-modified oligonucleotides have the major advantage over their 5′-analogues to exhibit a much greater nuclease stability.[30] The effect of the oxidizing property of this $[Ru(tap)_3]^{2+}$ complex appears also at the level of the AT sequences, for which the photocrosslinking becomes possible despite the lower reduction power of the adenine relative to that of the guanine units of the target strand. In conclusion, the data reported here should pave the way to a better design of Ru–ODNs conjugates as potential candidates for DNA sequence-specific damaging agents.

Experimental Section

General: The synthesis and purification of $[Ru(tap)_2phen"]^{2+}$ and $[Ru(tap)_2tap"]^{2+}$, the preparation of the oligonucleotides and the coupling procedures have been reported earlier.[20,28] The mass of the single-strand metallated oligonucleotides was measured by MALDI-TOF. Mass spectra were recorded with a Biflex Bruker spectrometer. The conjugates were dissolved in $CH_3CN/H_2O/NEt_3$ (50:50:2) with CH_3CN/H_2O (50:50) as eluent. Respectively, as single-strand conjugate, calcd. mass ($g\,mol^{-1}$), found mass $[M - H]^-$ RuT_2P-5′-0, 6091.2, 6090.4; RuT_2P-5′-1, 6061.5, 6061.7; RuT_2P-3′-0, 6049.1, 6050.3; RuT_2P-3′-1, 6019.2, 6020.7; RuT_3-5′-0, 6093.5, 6091.9; RuT_3-5′-1, 6063.5; 6061.8; RuT_3-3′-0, 6051.3, 6052.6; RuT_3-3′-1, 6027.2, 6028.5. The concentrations of the metallated oligonucleotides were determined optically by using the absorption coefficient value ε given in the literature for the free complexes.[22,29] The concentration of the complementary strands was determined by using the absorption coefficient value ε at 260 nm (complementary strand to sequence 0 and 1, ε = 205600 $M^{-1}cm^{-1}$ and 199300 $M^{-1}cm^{-1}$, respectively). The duplex solutions were prepared from equimolar single-strand solutions in aqueous buffer (50 mM NaCl, 10 mM Tris, pH 7). The Tris-HCl buffer (1 M, pH 7) stock standard solution was purchased from Sigma, and the water was purified by using a Millipore Milli-Q system.

Spectroscopy: Absorption and emission spectra were recorded at room temperature. Absorption spectra were monitored with a Perkin–Elmer Lambda UV/Vis spectrophotometer. Emission spectra were recorded with a Shimadzu RF-5001PC spectrofluorimeter equipped with a Hamamatsu R928 red-sensitive photomultiplier tube. The spectra were corrected for the instrument response. Emission lifetimes were determined by single-photon counting (SPC) with an Edinburgh Instruments FL900 spectrometer (Edinburgh Instruments, UK) equipped with a nitrogen-filled discharge lamp and a Peltier-cooled Hamamatsu R995 photomultiplier tube. The emission decays were analyzed by using the original Edinburgh Instruments software.

Steady-State Illuminations: Ru-ODN duplex photolyses were carried out in a 600 μL quartz cell (1.0 × 0.2 cm) with visible light (λ > 400 nm) from two lamps perpendicular to each other. The first source was a quartz halogen lamp (Philips 2000 W) and the second was a super-pressure mercury lamp (Osram HBO 200 W). Water was allowed to circulate through a filter to cut off the IR radiation, and a 0.2 M $NaNO_2$ solution was used to remove the UV part of the source. Absorption spectra were recorded with a Perkin–Elmer Lambda UV/Vis spectrophotometer.

Gel Electrophoresis: The target oligonucleotides were 5′-end-labelled by T4 polynucleotide kinase by using [γ^{32}P]-ATP 3000 Ci mmol^{-1} (Amersham) at 37 °C for 30 min. The addition of 5 μL of a 10% aqueous EDTA solution stopped the kinase activity. Excess ATP and kinase were removed by exclusion chromatography with Micro Bio-Spin P6 in Tris buffer (Bio-Rad). The duplex solutions (8 μM) were prepared by mixing equimolar solutions of the Ru–oligonucleotides and complementary single-strand oligonucleotides in 10 mM Tris-HCl buffer, 50 mM NaCl (pH 7). Those solutions were heated to 80 °C for 5 min before cooling down slowly for homogeneous hybridization. The duplex solutions were illuminated at 442 nm at room temperature with a monochromatic laser (He-Cd, 50 mW, Melles Griot). The loading buffer (89 mM Tris-HCl, pH 8.0, 89 mM boric acid, 2 mM EDTA, 7 M urea, 12% Ficoll, 0.02% xylene cyanol, 0.01% bromophenol) was then added in the samples. The ODN products were separated by electrophoresis on polyacrylamide gel (20% with a 19:1 ratio of acrylamide/bisacrylamide) containing urea (7 M) in TBE buffer (90 mM Tris-borate, pH 8, 2 mM EDTA). ODN fragments were visualized by autoradiography with Phosphor Screen and were counted with a phosphorimager Storm 860 instrument.

Mass Spectrometry: Solutions of the RuT_2P-3′-0 and RuT_3-3′-1 duplexes (V = 100 μL, C = 10 μM in 10 mM Tris-HCl buffer, 50 mM NaCl, pH 7) were prepared then heated at 85 °C for 10 min before cooling down slowly. RuT_3-3′-1 was then illuminated at 442 nm for 1 h with a monochromatic laser (He-Cd, 50 mW, Melles Griot), whereas RuT_2P-3′-0 was kept in the dark. The samples were diluted to 400 μL with water and dialyzed against water to remove NaCl (cellulose membrane, MWCO = 3500). Water was then evaporated with a speed-vac, and the residues were dissolved in a 1:1 acetonitrile/ammonium acetate (5 mM) mixture (denaturing conditions) to achieve ca. 50 μM concentrations. Fresh solutions were immediately subjected to mass spectrometry analysis. The mass spectrometry measurements were performed with a Waters QToF2 apparatus equipped with an orthogonal nanoelectrospray ionization (nano-ESI) source (Z-spray) operating in positive ion mode. Sample solutions were directly infused into the ESI source from Proxeon NanoES capillaries. Typical ESI conditions were capillary voltage 1.2 kV, cone voltage 80 V, extractor voltage 5 V, source temperature 80 °C and desolvation temperature 120 °C. Dry nitrogen was used as the ESI gas. The quadrupole was set to pass ions from 100 to 3000 Th and all the ions were transmitted into the pusher region of the time-of-flight analyzer for mass analysis with 1 s integration time. The data were acquired in continuum mode until acceptable average data were obtained.

Supporting Information (see footnote on the first page of this article): Absorption spectra of $[Ru(tap)_2phen"]^{2+}$ and $[Ru(tap)_2tap"]^{2+}$ under visible irradiation; absorption spectra of the RuT_2P-3′-1 and RuT_3-3′-1 duplexes under visible irradiation; mass spectrometry analysis of the RuT_2P-3′-0 duplex.

Acknowledgments

The authors thank the Belgian Science Policy (program IAP, P6/27) and the FRFC-FNRS for financial support. They are also grateful to the COST D35 program for collaborations. S.D. thanks the FRIA (Fonds pour la Recherche dans l'Industrie et l'Agriculture) for a fellowship. The authors are also grateful to the NanoBio

program for the facilities of the Synthesis Platform and the Région Rhône-Alpes for financial support. The Mons laboratory thanks the "Fonds National de la Recherche Scientifique" for its contribution to the acquisition of the Waters QToF2 mass spectrometer. P.G. (FRS-FNRS Research Associate) is also grateful to the FRS-FNRS for continuing support.

[1] a) N. Dias, C. A. Stein, *Mol. Cancer Ther.* **2002**, *1*, 347–355; b) D. D. Ma, T. Rede, T. A. Naqui, P. D. Cook, *Biotechnol. Annu. Rev.* **2000**, *5*, 155–196; c) S. T. Crooke, *Annu. Rev. Med.* **2004**, *55*, 61–95.

[2] A. Bochot, P. Couvreur, E. Fattal, *Prog. Retinal Eye Res.* **2000**, *19*, 131–147.

[3] D. A. Braasch, D. R. Corey, *Biochemistry* **2002**, *41*, 4504–4510.

[4] M. B. Gottikh, O. A. Fedorova, M.-V. Baud-Demattei, S. Giorgi-Renault, J.-R. Bertrand, Z. A. Shabarova, C. Malvy, *J. Am. Chem. Soc.* **1996**, *118*, 2126–2130.

[5] C. Cazenave, M. Chevrier, N. T. Thuong, C. Hélène, *Nucleic Acids Res.* **1987**, *15*, 3421–3437.

[6] S. L. Loke, C. A. Stein, X. H. Zhang, K. Mori, M. Nakanishi, C. Subasinghe, J. S. Cohen, L. M. Neckers, *Proc. Natl. Acad. Sci. USA* **1989**, *86*, 3474–3478.

[7] L. A. Yabukov, E. A. Deeva, V. F. Zarytova, E. M. Ivanova, A. S. Ryte, L. V. Yurchenko, V. V. Vlassov, *Proc. Natl. Acad. Sci. USA* **1989**, *86*, 6454–6458.

[8] J. Kurreck, *Eur. J. Biochem.* **2003**, *270*, 1628–1644.

[9] M. D. Hugues, M. Hussain, Q. Nawaz, P. Sayyed, S. Akhtar, *DDT* **2001**, *6*, 303–315.

[10] M. Manoharan, *Antisense Nucleic Acid Drug Dev.* **2002**, *12*, 103–128.

[11] a) R. L. Juliano, *Curr. Opin. Mol. Ther.* **2005**, *7*, 132–136; b) N. Venkatesan, B. H. Kim, *Chem. Rev.* **2006**, *106*, 3712–3761.

[12] T. Da Ros, G. Spalluto, M. Prato, T. Saison-Behmoaras, A. Boutorine, B. Cacciari, *Curr. Med. Chem.* **2005**, *12*, 71–88.

[13] J.-P. Lecomte, A. Kirsch-De Mesmaeker, M. M. Feeney, J. M. Kelly, *Inorg. Chem.* **1995**, *34*, 6481–6491.

[14] H. Uji-i, P. Foubert, F. De Schryver, S. De Feyter, E. Gicquel, A. Etoc, C. Moucheron, A. Kirsch-De Mesmaeker, *Chem. Eur. J.* **2006**, *12*, 758–762.

[15] L. Jacquet, D. R. Davies, A. Kirsch-De Mesmaeker, J. M. Kelly, *J. Am. Chem. Soc.* **1997**, *119*, 11763–11768.

[16] a) L. Herman, S. Ghosh, E. Defrancq, A. Kirsch-De Mesmaeker, *J. Phys. Org. Chem.* **2008**, *21*, 670–681 and references cited therein; b) In review, the exergonicity of the electron transfer from the guanine base mononucleotide to the excited complex according to the Rehm–Weller equation is discussed; it is either –0.07 or –0.25 eV for $[Ru(tap)_3]^{2+}$ and either + 0.12 or –0.06 eV for $[Ru(tap)_2phen]^{2+}$. This depends on the value of the oxidation potential chosen for G from the literature. The most exergonic process (–0.07 and –0.25 eV) is obtained with the oxidation potential determined from radiolysis experiments, that is, corresponding to a proton-coupled electron transfer (PCET). Therefore, it is probable, as shown by picosecond laser experiments, that the quenching corresponds to a PCET.

[17] H. C. Kolb, M. G. Finn, K. B. Sharpless, *Angew. Chem. Int. Ed.* **2001**, *40*, 2004–2021.

[18] P. M. E. Gramlich, C. T. Wirges, A. Manetto, T. Carell, *Angew. Chem. Int. Ed.* **2008**, *47*, 8350–8358.

[19] Y. Singh, N. Spinelli, E. Defrancq, *Curr. Org. Chem.* **2008**, *12*, 263–290 and references cited therein.

[20] M. Villien, S. Deroo, E. Gicquel, E. Defrancq, C. Moucheron, A. Kirsch-De Mesmaeker, P. Dumy, *Tetrahedron* **2007**, *63*, 11299–11306.

[21] a) A. Del Guerzo, A. Kirsch-De Mesmaeker, M. Demeunynck, J. Lhomme, *J. Phys. Chem. B* **1997**, *101*, 7012–7021; b) R. Blasius, *Thèse de doctorat*, Université libre de Bruxelles, **2003**.

[22] A. Masschelein, L. Jacquet, A. Kirsch-De Mesmaeker, J. Nasielski, *Inorg. Chem.* **1990**, *29*, 855–860.

[23] For biexponential decays, if one of the lifetimes is not at least the double of the other one, a full confidence into the lifetime values cannot be given. If triexponential decay functions are needed for fitting the results, which is generally the case with such systems when a luminescence quenching is present, it is probable that only the extreme lifetimes (the longest and the shortest ones) are significant.

[24] E. R. Carraway, J. N. Demas, B. A. DeGraff, *Anal. Chem.* **1991**, *63*, 332–336.

[25] With $[Ru(tap)_3]^{2+}$, we cannot determine the percentage of quenching inside the RuT_3-5′-1 ODN duplex as performed for $[Ru(tap)_2phen]^{2+}$, because the RuT_3-5′-0 duplex already presents a slight quenching and thus cannot play the role of reference.

[26] D. García-Fresnadillo, N. Boutonnet, S. Schumm, C. Moucheron, A. Kirsch-De Mesmaeker, E. Defrancq, J.-F. Constant, J. Lhomme, *Biophys. J.* **2002**, *82*, 978–987.

[27] C. W. Crean, Y. T. Kavanagh, C. M. O'Keeffe, M. P. Lawler, C. Stevenson, R. J. H. Davies, P. H. Boyle, J. M. Kelly, *Photochem. Photobiol. Sci.* **2002**, *1*, 1024–1033.

[28] S. Deroo, V. Toncheva, E. Defrancq, C. Moucheron, E. Schacht, A. Kirsch-De Mesmaeker, *Biomacromolecules* **2007**, *8*, 3503–3510.

[29] I. Ortmans, B. Elias, J. M. Kelly, C. Moucheron, A. Kirsch-De Mesmaeker, *Dalton Trans.* **2004**, 668–676.

[30] D. A. Stetsenko, M. J. Gait, *Bioconjugate Chem.* **2001**, *12*, 576–586.

Received: November 5, 2008
Published Online: December 19, 2008

